Polymer Chemistry

Accepted Manuscript

This article can be cited before page numbers have been issued, to do this please use: S. Subramaniyan, A. Hindi, F. Guerrero-Ruiz and M. Hakkarainen, *Polym. Chem.*, 2026, DOI: 10.1039/D6PY00244G.

ROYAL SOCIETY OF CHEMISTRY

rsc.li/polymers

View Article Online
DOI: 10.1039/D6PY00244G

Recycling Post-Consumer Polyesters Bottles and Fabrics to Photocurable Covalent Adaptable networks

Sathiyaraj Subramaniyan,[1] Amro Hindi,[1] Federico Guerrero-Ruiz,[1,2] Minna Hakkarainen[1,2]*

[1]*Department of Fibre and Polymer Technology, KTH Royal Institute of Technology, Teknikringen 58, 100 44 Stockholm, Sweden.*

[2] *Wallenberg Initiative Materials Science for Sustainability, KTH Royal Institute of Technology, Teknikringen 58, 100 44 Stockholm, Sweden.*

**Email: minna@kth.se*

View Article Online
DOI: 10.1039/D6PY00244G

Abstract

Recycling aromatic polyester waste into UV-curable covalent adaptable networks (CANs) offers a promising pathway toward more circular materials. Here, we present a straightforward strategy to convert post-consumer polyethylene terephthalate (PET) bottles and polybutylene terephthalate (PBT) fabrics into photocurable, mechanically reprocessable, and chemically degradable CANs. PET and PBT were first depolymerized via glycolysis or alcoholysis to yield BHET and BHBT, which were subsequently methacrylated to form resins PR and FR. A third resin, SBJR, containing dynamic imine (Schiff-base) linkages, was synthesized from methacrylated vanillin and Jeffamine to introduce reversible bonding into the network. These components enabled fabrication of two permanently crosslinked polymers (PR100, FR100) and two covalent adaptable networks (CAN1, CAN2). Structural analysis verified the expected chemical transformations, and all materials exhibited good thermal stability, with CANs showing slightly reduced $T_{5\%}$ due to flexible aliphatic segments and reversible imine bonds. Rheological creep and stress-relaxation studies supported associative imine exchange as the governing mechanism without network dissociation. CAN2 also demonstrated robust solvent resistance and could be mechanically recycled and chemically degraded through imine-exchange-driven depolymerization. Overall, this work establishes an efficient molecular design framework for transforming plastic and textile waste into photocurable materials, advancing value of plastic waste as a resource for new materials and reduced environmental pollution.

View Article Online
DOI: 10.1039/D6PY00244G

Introduction

Plastic pollution is widely recognized as a major global environmental challenge.[1–3] Among synthetic polymers, polyethylene terephthalate (PET) and polybutylene terephthalate (PBT) rank among the most heavily produced materials, representing roughly 6% of worldwide plastic production and increasing annually due to extensive use in packaging, textiles, construction, and electronics.[4,5] The attractive thermoplastic properties - high mechanical strength, optical transparency, and processability[2,6] – also contribute to their persistence in the environment, generating long-term ecological impacts in the absence of effective end-of-life solutions.[7–10] To address this, numerous chemical recycling routes have been developed, including glycolysis,[11,12] hydrolysis,[13] ammonolysis,[13–15] acidolysis, and alcoholysis. Several of these have advanced to commercial implementation,[16,17] reflecting increased efforts to close the material loop and reduce dependence on virgin fossil-derived feedstocks.[10,18,19]

Recently, Liu *et. al*., reported a strategy for constructing closed-loop recyclable polymer aerogels derived from low-cost PET waste,[20] while Feng *et. al*., developed an effective approach to upcycle PET into closed-loop recyclable carbon-fiber-reinforced polymer composites (CFRPCs) with high mechanical performance (Scheme 1).[10] Singh *et. al*., further reported upcycling of PET waste into poly(ester-amide) capable of closed-loop circularity.[6] In addition, Jia *et al.,* investigated recycling of PET into polyester-based covalent adaptable networks (CANs) with varying network densities.[21]

The depolymerization of PET via glycolysis is promoted by catalysis. A wide range of catalysts has been employed, such as zinc acetate ($Zn(OAc)_2$), 1,5,7-triazabicyclo[4.4.0]dec-5-ene (TBD), sodium methoxide (NaOMe), carbonate bases ($NaHCO_3$, Na_2CO_3, and $CaCO_3$, etc.), as well as heterogeneous organic catalysts such as MOF or COF.[22–24] These catalysts improve

View Article Online
DOI: 10.1039/D6PY00244G

transesterification efficiency and accelerate PET breakdown.[25–29] In addition, ionic liquids (ILs) and deep eutectic solvents (DESs) have emerged as promising alternatives, acting simultaneously as reaction media and catalysts to improve glycolytic efficiency and bis(2-hydroxyethyl) terephthalate (BHET) yields.[4] Li *et al.* demonstrated that PET-derived polyurethane elastomers can be synthesized via DES-assisted glycolysis,[30] while Ha *et al.* and Attallah *et al.* showed that microwave-assisted DES glycolysis enables rapid, high-yield depolymerization. Bifunctional DESs can further deliver high monomer recovery under relatively mild conditions.[31,32] Despite these advances, challenges remain—including catalyst separation, BHET purification, and managing mixed-waste streams. Yet, when combined with greener catalysts and energy-efficient technologies, glycolysis remains one of the most promising pathways for scalable PET chemical recycling and industrial adoption.[28,29]

Covalent adaptable networks (CANs) are cross-linked polymers capable of altering their network topology through associative or dissociative bond-exchange reactions. These materials combine the mechanical, thermal, and solvent resistance of thermosets with the reprocessability typically associated with thermoplastics. Incorporating imine bonds into CANs introduces dynamic exchange pathways—including transimination, imine metathesis, and imine hydrolysis—and these networks can be readily synthesized by condensing aldehydes or ketones with amines.[18,33–35] The presence of imine linkages imparts potential for thermal reprocessability, chemical recyclability, self-healing, and shape memory capabilities.[36,37,38] Existing PET-upcycling studies largely focused on depolymerization to BHET followed by conversion into thermoplastics, with only a limited number demonstrating the transformation of PET into dynamically crosslinked polymers (Scheme 1).[39–41] Moreover, these examples typically relied on multistep workflows.[3,21,42] Beyond CAN formation, broader research shows that PET recycling can yield

View Article Online
DOI: 10.1039/D6PY00244G

epoxy resins, alkyd resins, coatings, and other high-value materials, further highlighting the significant potential of polyester waste as a circular feedstock.[8]

Here, we test the hypothesis that post-consumer PET bottles and PBT textile waste can be depolymerized and used as raw materials for UV-curable covalent adaptive networks (CANs). We introduce a recycling route that couples alcoholytic depolymerization, methacrylation, and dynamic-imine network design to generate mechanically reprocessable and chemically degradable CANs from waste-derived monomers. The resulting materials were comprehensively evaluated from mechanical performance and stress relaxation behavior to recyclability. This strategy provides a promising approach to develop more circular resin systems and offers a basis for future research on scalable pathway.

View Article Online
DOI: 10.1039/D6PY00244G

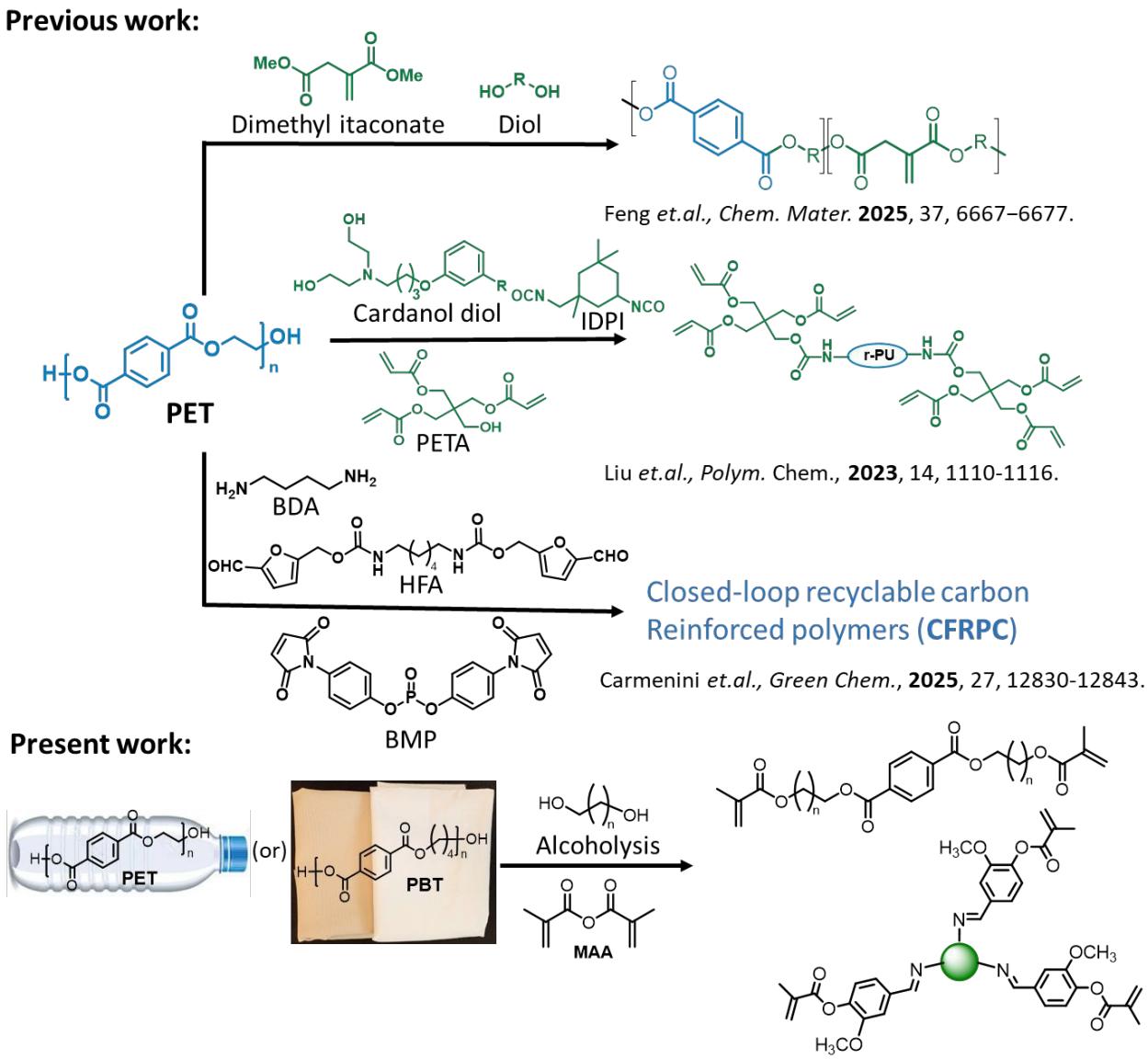

Scheme 1. Comparison of photocurable resins previously formulated from alcoholysis products of PET and in current work also from alcoholysis of PBT fabrics.

Results and discussion

Synthesis of photocurable resins from post-consumer bottles and fabrics

Commercial PET bottles and PBT fabrics were chemically depolymerised to be utilized as photocurable resin components (Scheme 2). In the first step, the materials were uniformly cut into small pieces, which were subjected to chemical depolymerization through reaction with ethylene glycol or 1,4-butanediol, respectively, in the presence of zinc acetate ($Zn(OAc)_2$) as a catalyst to obtain their

View Article Online
DOI: 10.1039/D6PY00244G

corresponding alcoholysis products, **BHET** and **BHBT**. Subsequently, in the presence of dimethyl aminopyridine (DMAP) as a catalyst, BHET and BHBT underwent a methacrylation reaction with methacrylic anhydride to generate the photocurable resins, **PR** and **FR**. A third resin component containing a dynamic imine-bonds (Schiff base) to facilitate circularity was synthesized starting from Jeffamine and biobased methacrylated vanillin (SBJR) (Scheme 2). These three photocurable resins were then formulated into two traditional thermosetting polymers (**PR100** and **FR100**) and two covalent adaptable networks (**CAN1** and **CAN2**) shown in Scheme 2.

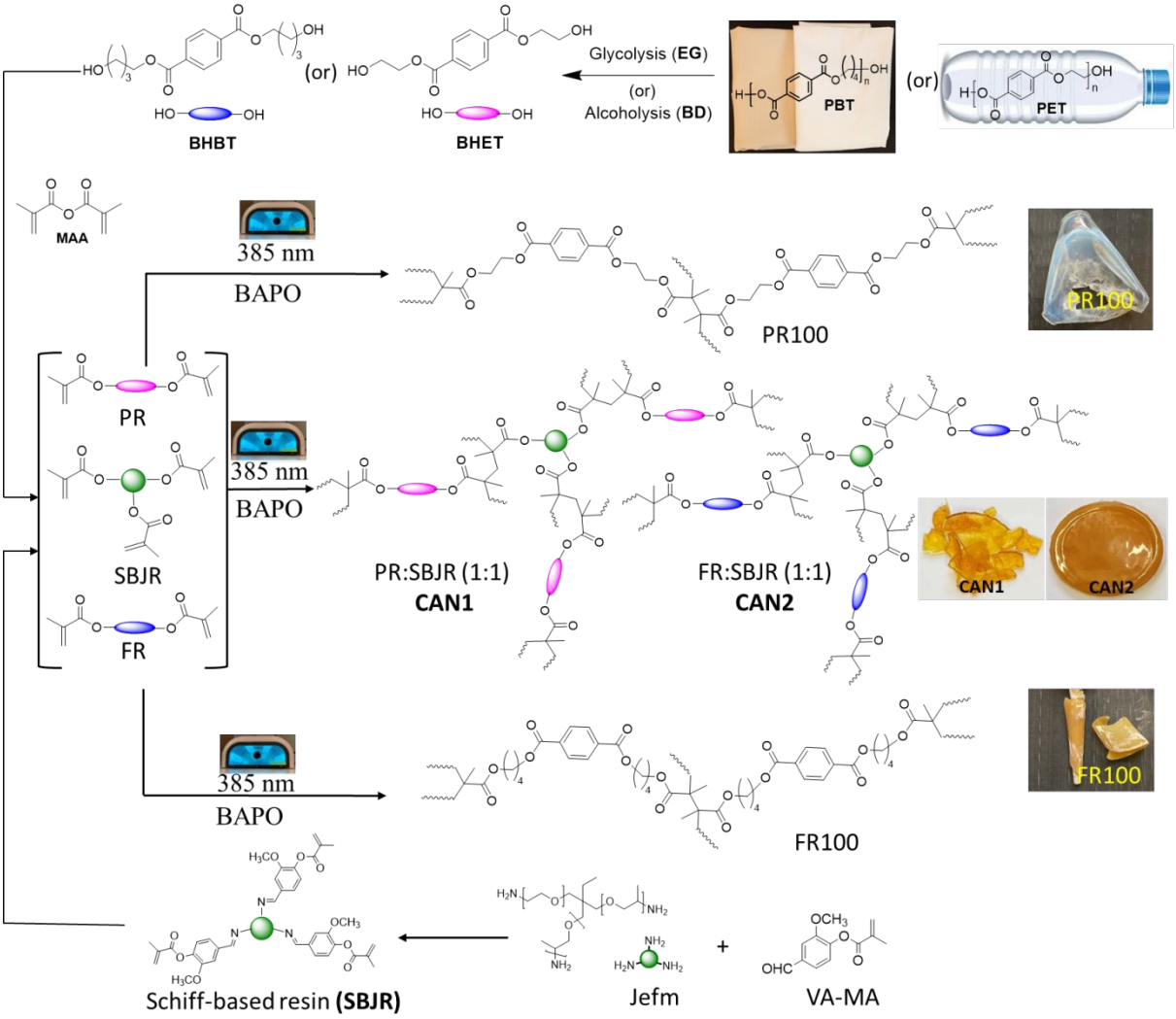

View Article Online
DOI: 10.1039/D6PY00244G

Scheme 2. The synthesized photocurable resins, and photocured thermosets (**PR100 and FR100**) and covalent adaptable networks (**CAN1** and **CAN2**).

The chemical structures of the intermediates and resins were confirmed by NMR. In the ^{1}H NMR spectra of intermediates BHET and BHBT, the peaks of ester-CH_2 and aliphatic-OCH_2 appeared at δ ~4.52 and 4.01 ppm, respectively, and the aromatic signal appeared at δ 8.15 ppm. Similarly, in BHBT, the peaks of ester-CH_2 and aliphatic-OCH_2 appeared at δ ~4.51 to 4.63 ppm, the peak of aliphatic-CH_2 appeared at δ ~1.74 to 1.93 ppm, and the peak of aromatic-CH appeared at δ 8.11 ppm. After methacrylation, due to the electron-withdrawing properties of the vinyl ester group, the BHET and BHBT of the ester and aliphatic -OCH_2 shifted slightly to the up-field, and three new peaks were observed at δ~6.15 and 5.61 ppm, and δ 1.96 ppm, respectively, corresponding to the methacrylic -CH_2 and -CH_3 peaks. The other peaks, such as the ester -CH_2 and aliphatic -OCH_2, aliphatic -CH_2 and aromatic signals, correspond well with the photocurable resins (**PR** and **FR**) (Figure 1A). In the ^{1}H NMR spectrum of SBJR, methacrylate hydrogen peaks appeared at δ 5.90, 6.27, and 1.98 ppm, which agrees with previously reported SBJR spectra.[34]

In ^{13}C NMR spectra of BHET and BHBT, aromatic ester carbonyl and aromatic carbons, aliphatic -OCH_2 and -CH_2 peaks were observed at δ ~165.63, 134,10-129.52, 67.49-59.44 and ~29.15 ppm, respectively. After the methacrylation vinyl and aromatic ester carbonyl peaks were observed at δ ~167.12, 165.48, aromatic and methacrylic carbons, aliphatic -OCH_2 peaks appeared at δ ~135.88 to 62.25 ppm, and methacrylic -CH_3 peak at δ ~18.26 ppm as shown in Figure 1B. All shifts in ^{13}C NMR spectra of FR unambiguously matched with the structure (Figure S2), while the spectrum of SBJR was again consistent with the spectrum previously reported in the literature.[34]

View Article Online
DOI: 10.1039/D6PY00244G

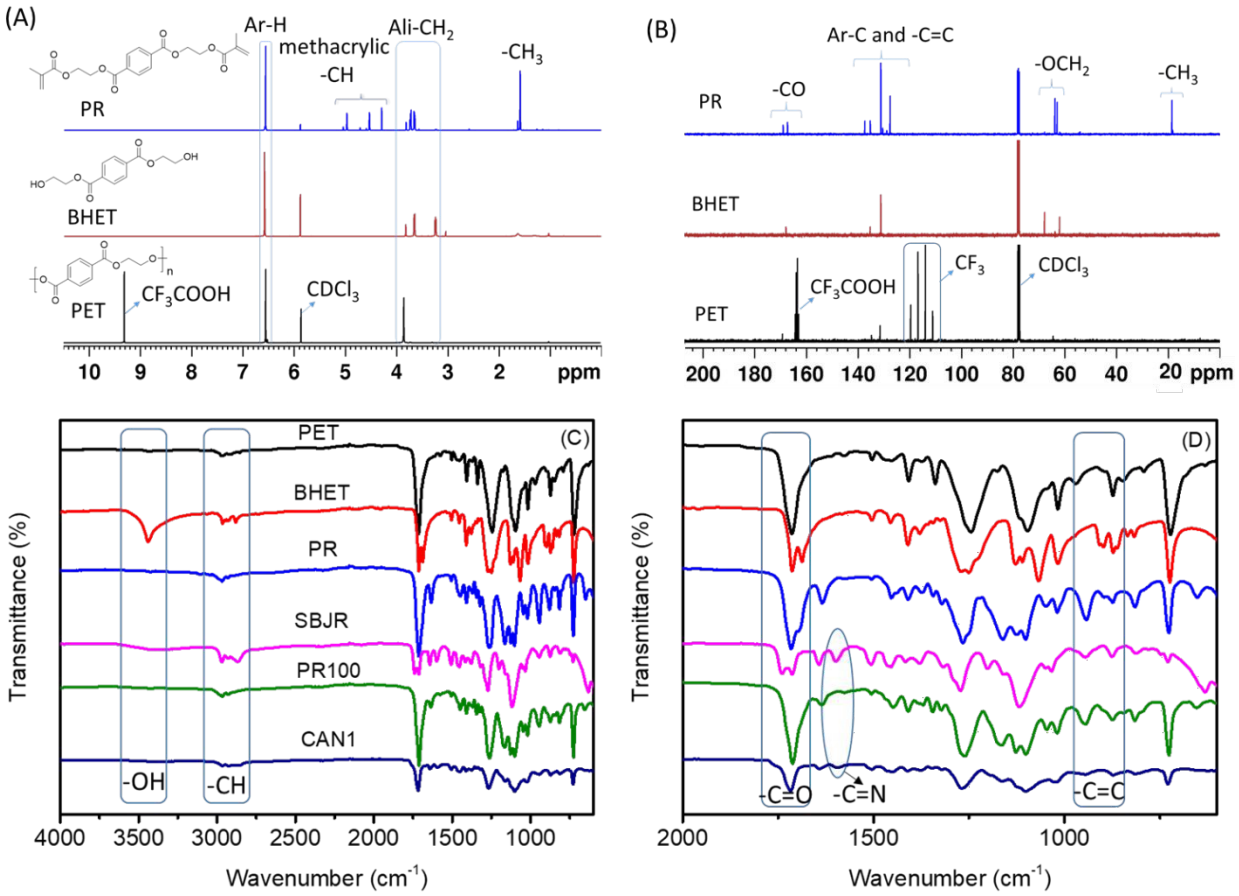

Figure 1. (A) ^{1}H NMR (400.13 Hz, *CDCl$_3$*) and (B) ^{13}C NMR (100.61 MHz, *CDCl$_3$*) spectra of PET, BHET and PR. (C and D) FTIR spectra of PET, BHET, PR, SBJR, PR100 and CAN1.

The structures of the photocurable resins (PR, FR and SBJR) and corresponding cross-linked materials (PR100, FR100, CAN1 and CAN2) were also confirmed by FTIR analysis (Figure 1C-D and Figure S3 A-B). For the resins, ester carbonyl stretching signals were observed at ~1715 cm^{-1}, imine (-C=N) peaks at ~1605 cm^{-1}, and -C=C bending vibrational peaks at ~941 and 876 cm^{-1}, respectively. After photopolymerization the intensity of -C=C bending vibrational peaks decreased at ~941 and 876 cm^{-1} indicating consumption of methacrylate bonds in the photopolymerization reaction, while the remaining peaks exactly matched with corresponding polymer structures.

View Article Online
DOI: 10.1039/D6PY00244G

Thermal properties

Thermogravimetric analysis (TGA) was used to analyse the thermal stability of intermediates, photocurable resins, and the final photocured crosslinked polymers, see Figure 2, Figure S4 and Table S1. Uncured resins PR and FR demonstrated $T_{5\%}$ of 214 °C and 181 °C, respectively, and the maximum decomposition temperatures (T_d) were observed at 424 °C and 409 °C (Figure 2A, Table S1). The $T_{5\%}$ and T_d of uncured Schiff-base resin (SBJR) were in the same range, *i.e.,* 215 °C and 394 °C, respectively. After crosslinking the thermal stability of PR100 and FR100 significantly increased, resulting in $T_{5\%}$ values of 264 °C and 221 °C. These values are approximately ~40-50 °C higher than the corresponding values for uncured resins (PR and FR). The $T_{5\%}$ and T_d of FR and FR100 were somewhat lower than those observed for PR and PR100, which is explained by the longer aliphatic alcohol, resulting also in slightly lower aromatic content. Mixing SBJR with PR or FR to prepare crosslinked CAN1 and CAN2, resulted in T_5 of 221 °C and 187 °C, *i.e.,* a reduction of approximately 30-40 °C compared to PR100 and FR100, which could be explained by the introduction of flexible aliphatic Jefm units and labile imine-bonds. However, the T_d values were similar to values of PR100 and FR100. While these $T_{5\%}$ values were slightly lower than what has been reported for similar systems earlier, the T_d values were in the same range. As an example, one-pot depolymerization of PET waste into photocurable resins led to $T_{5\%}$ and T_d values of ~329-365 ℃ and ~366-414 ℃,[6,10] while vanillin-containing Schiff base-based photocurable networks had $T_{5\%}$ and T_d values from 250-270 ℃ and ~410 ℃, respectively. [34,43]

View Article Online
DOI: 10.1039/D6PY00244G

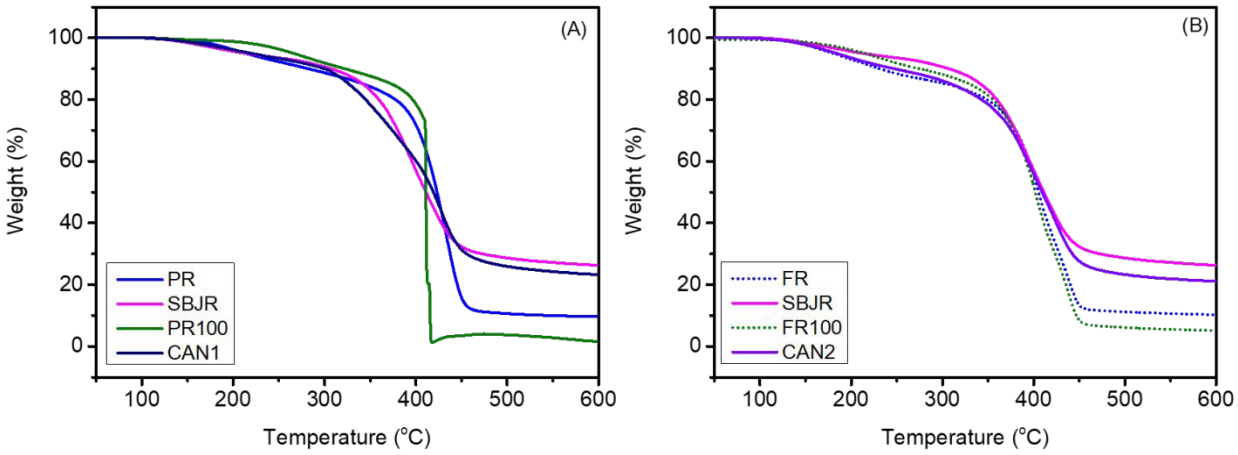

Figure 2. TGA analysis of (A) PET bottle derived intermediates, photocured PR100 and CAN1 and (B) PBT fabric derived intermediates, photocured FR100 and CAN2.

Thermomechanical analysis

Thermomechanical properties of the thermosets (PR100 and FR100) and CANs (CAN1 and CAN2) were analyzed by dynamic mechanical analysis (DMA) (Figure S5 and Table-S1). The T_g were determined from *tan δ* curves. PR100 and FR100, exhibited relatively high T_g values (202 ℃, 154 ℃, respectively), while T_g values of corresponding CAN1 and CAN2 with flexible Jefm were significantly lower (128 ℃ and 52 ℃, respectively). Broadening of the *tan δ* curves, especially in the case of FR100 and CAN1, is attributed to the heterogeneity of the cross-linked materials. These values are significantly higher than the previously reported T_g (25 °C) for CANs prepared by photocuring SBJR alone in the absence of PR100 or FR100.[34] This is explained by the higher rigidity and aromatic content compared to the flexible SBJR.

Furthermore, the crosslinking densities of thermosets (PR100, FR100), and CAN1 and CAN2 were calculated as 1.8 x 10^3, 1.6 x 10^3, 6.4 x 10^3 and 2.8 x 10^3 mol/m^3 and the storage moduli at 30 °C were ~18, 16, 57, and 2.5 MPa, respectively. Both traditional thermosets illustrated relatively similar crosslinking densities and storage moduli, while CAN1 exhibited higher

View Article Online
DOI: 10.1039/D6PY00244G

crosslinking density and storage modulus. The crosslinking density of CAN2 was intermediate between thermosets and CAN1, while it had the lowest storage modulus. The lower crosslinking density of CAN2 compared to CAN1, agrees with observed lower gel content and solvent stability (Table S2) with possible additional influence from the longer alcohol used during depolymerization. The significantly lower storage modulus of CAN2 observed at 30 ^{o}C is likely mainly deduced to the closeness to T_g with further contribution from the more flexible structure and lower crosslinking density compared to CAN1.

In addition, thermomechanical analysis of CAN1 and CAN2 was performed using rheology through three different types of experiments shown in Figure 3 A-D and S6. This analysis is approximately three orders of magnitude more sensitive than calorimetric analysis for detecting T_g, and it allowed determination of T_g of CAN1 and CAN2 at 103 and 83 °C, respectively. The lower T_g, of CAN2 was expected due to the greater structural flexibility of BHBT compared to BHET. It is also expected that the T_g, obtained by thermomechanical analysis is somewhat higher compared to the one obtained by calorimetric analysis. No dissociation was observed in the storage modulus within the rubbery state, at least up to 200 °C, supporting an associative exchange mechanism.

Creep tests were conducted at different temperatures, all at least 50 °C above the highest T_g, and below $T_{5\%}$ obtained by TGA: i.e., at 160, 170 and 180 °C. An interesting effect was observed: although both materials exhibited creep deformation due to the presence of imine bonds, the influence of temperature appeared to be minimal. As a result, parameters such as the activation energy (E_a) and the topology freezing transition temperature (T_v) could not be reliably extracted

View Article Online
DOI: 10.1039/D6PY00244G

from these experiments. Nevertheless, this behaviour is promising. The limited influence of temperature on the strain-time response suggests a high crosslinking density, leaving little free volume available for network rearrangement. Additionally, stresses higher than 75 000 Pa could not be applied due to instrument overspeed limitations.

Finally, stress relaxation tests were performed at 160 ºC, 170 ºC and 180 °C on both CAN1 and CAN2. The relaxation times ($\tau_{37}\%$) were only around one minute, confirming again the dynamic behaviour facilitated by the imine bonds. Unfortunately, it was not possible to accurately determine E_a and T_v due to the lack of a stable storage modulus at rubbery plateau. Consequently, stress relaxation measurements were only performed at a single temperature. After 30 minutes, no total relaxation was observed due to the highly crosslinked structure, remaining around 83 % relaxation for CAN1 and 91 % for CAN2. A higher relaxation in CAN2 was expected due to a lower T_g. Due to the absence of dissociation observed in the tan delta experiment, along with the existence of dynamism observed in the creep and stress relaxation experiments, we can conclude that the system is an associative adaptable covalent network (vitrimer), based on imine metathesis.

View Article Online
DOI: 10.1039/D6PY00244G

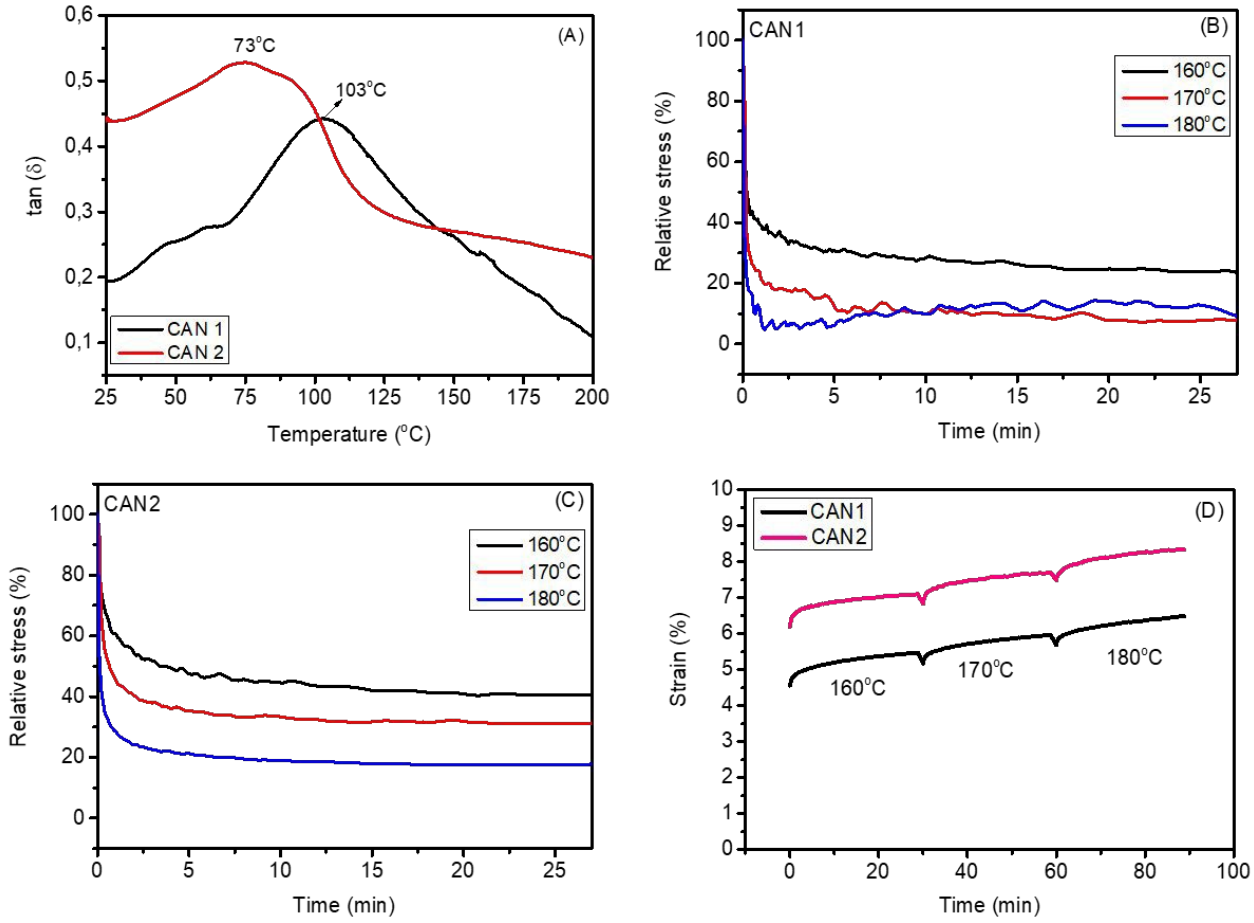

Figure 3. Rheological analysis showing (A) tan (δ) curves (B and C) CAN1 and CAN2 stress-relaxation curve at 160 °C, 170 °C and 180 °C and (D) creep test at 160 °C, 170 °C and 180 °C for CAN1 and CAN2.

Solvent resistance

Solvent resistance properties of CAN1 and CAN2 were analysed by immersing ~100 mg of the films into 5 mL of different solvents such as sodium hydroxide (1M NaOH), *N,N*-dimethylformamide (DMF), acetone (Ace), dimethyl sulfoxide (DMSO), tetrahydrofuran (THF), dichloromethane (DCM) and ethanol (EtOH), at room temperature for 2 days (Figure S7 and Table S2). Weight loss was measured after immersion in the solvents. Both CAN1 and CAN2

View Article Online
DOI: 10.1039/D6PY00244G

films remained intact in most solvents, and while CAN1 was generally more stable than CAN2. The exception was immersion in NaOH solution, which resulted in largest weight loss for both materials, possible due to hydrolysis of ester bonds in alkaline solution.[44] Surprisingly, these imine bond-containing CANs showed good stability in 1 M HCl solution due to the high crosslinking density confirmed by rheology, contrary to what is often observed for imine bond containing materials under acidic conditions (see Chemical degradation of CANs). This observation is also in agreement to what was observed for photocured SBJR in previous work.[43]

Mechanical reprocessability

Due to the known dynamic imine bond exchange reactions during heating, the network topology of CAN1 and CAN2 is expected to be able to rearrange endowing thermal reprocessability for the previously UV-cured films. The thermal reprocessability of UV-cured CAN1 and CAN2 was evaluated by cutting the materials into small pieces and placing them in a hot-press mold (180 ^{o}C, 200 kN for 15 min). These thermally reprocessed samples were denoted as CAN1 original and CAN2 original. Similar procedure was followed for the reprocessing cycle (second hot pressing). However, while CAN2 could be successfully reprocessed with adequate property retention, the reprocessed CAN1 films were too brittle for further use. The structural, thermal and mechanical properties of original and reprocessed materials were followed by FTIR, TGA and tensile testing (Figure 4 A-D and Table S1).

View Article Online
DOI: 10.1039/D6PY00244G

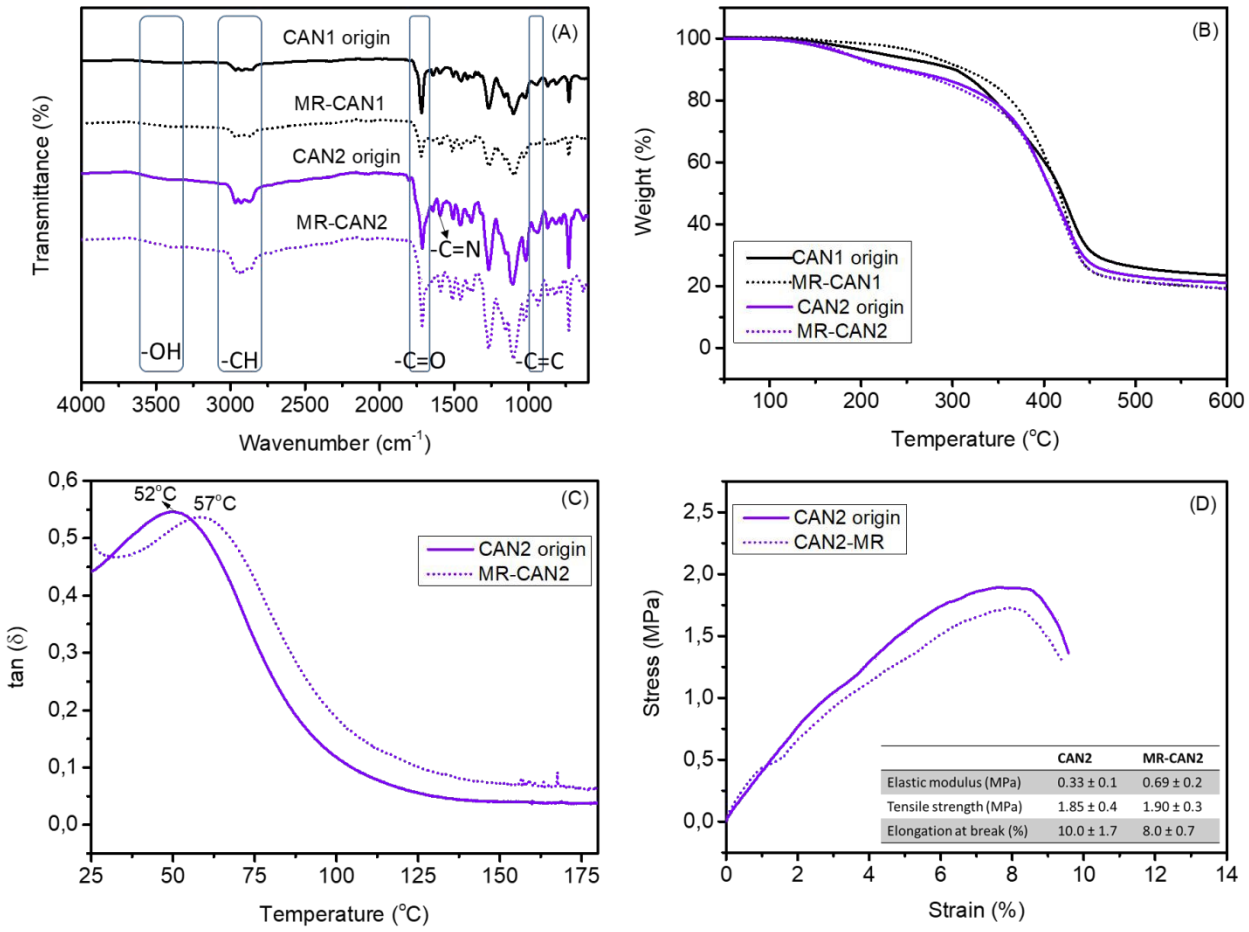

Figure 4. (A) FTIR spectra (B) TGA weight loss curves of original and mechanically reprocessed CAN1 and CAN2 (C) DMA tan (δ) curves and (D) Stress-strain properties of original and mechanically reprocessed CAN2.

In the FTIR spectra of once hot-pressed and reprocessed CAN1 and CAN2 all absorption bands (e.g., imine, ester, -C=C and -CH) matched the original spectra indicating no major structural changes. Furthermore, no deterioration of thermal stability was observed after reprocessing. For CAN1, T_d appeared at 405 °C and T_5 at 222 °C after reprocessing cycles (Figure 4B and Table S1). These values are very close to the original values of 403 °C and 221 °C, respectively. Similar was observed for CAN2. The influence of mechanical reprocessing on tensile properties of CAN2 was further analysed by tensile testing. After reprocessing the elastic modulus of

View Article Online
DOI: 10.1039/D6PY00244G

CAN2 increased from 0.33 MPa to 0.69 MPa and the tensile stress and elongation at break remained similar or slightly lower compared to the original values. Tensile testing of CAN1 was not performed due to the brittle nature of the material.

Chemical degradation

We previously reported recycling of linear and crosslinked Schiff base-based materials by immersion in an acidic aqueous solution (0.01 M HCl, pH ≈ 1) for 24 hours at room temperature.[18] The degradation rate increased with increasing HCl solution concentration (0.1 M and 1 M HCl) and temperature. Here, the chemical degradation of CAN2 was tested under increasingly acidic conditions (0.01 M, 0.1 M, and 1 M HCl (pH 0-2)), at room temperature and at 50 ^{o}C. However, CAN2 illustrated excellent chemical resistance in HCl solutions. Therefore, we further evaluated the chemical degradation of CAN2 by transimination in hexylamine (primary amine) in THF at 60 ^{o}C. After immersion in hexylamine/THF solution (1:4 mL) for 24 h at 60 ^{o}C, CAN2 fully dissolved (Figure 5A). A proposed degradation mechanism, where the excess of hexylamine caused an imine exchange reaction to occur is presented in Figure 5B and the ^{1}H NMR spectra of the organic layer at the beginning and after chemical degradation, as well as spectra of Jefm and SBJR is presented in Figure 5C. After the reaction of hexylamine with CAN2, the signal from the imine bond (δ ~8.30 ppm) connecting Jeffamine to the network disappeared, while the ^{1}H NMR spectrum of the crude dissolved product showed that a new imine (-C=N) peak appeared at δ ~8.10 ppm, supporting the transimination reaction. In addition, aromatic -CH peak appeared at δ ~6.75 to 7.30 ppm, and aliphatic -CH peak appeared at δ ~1.10 to 5.1 ppm.

View Article Online
DOI: 10.1039/D6PY00244G

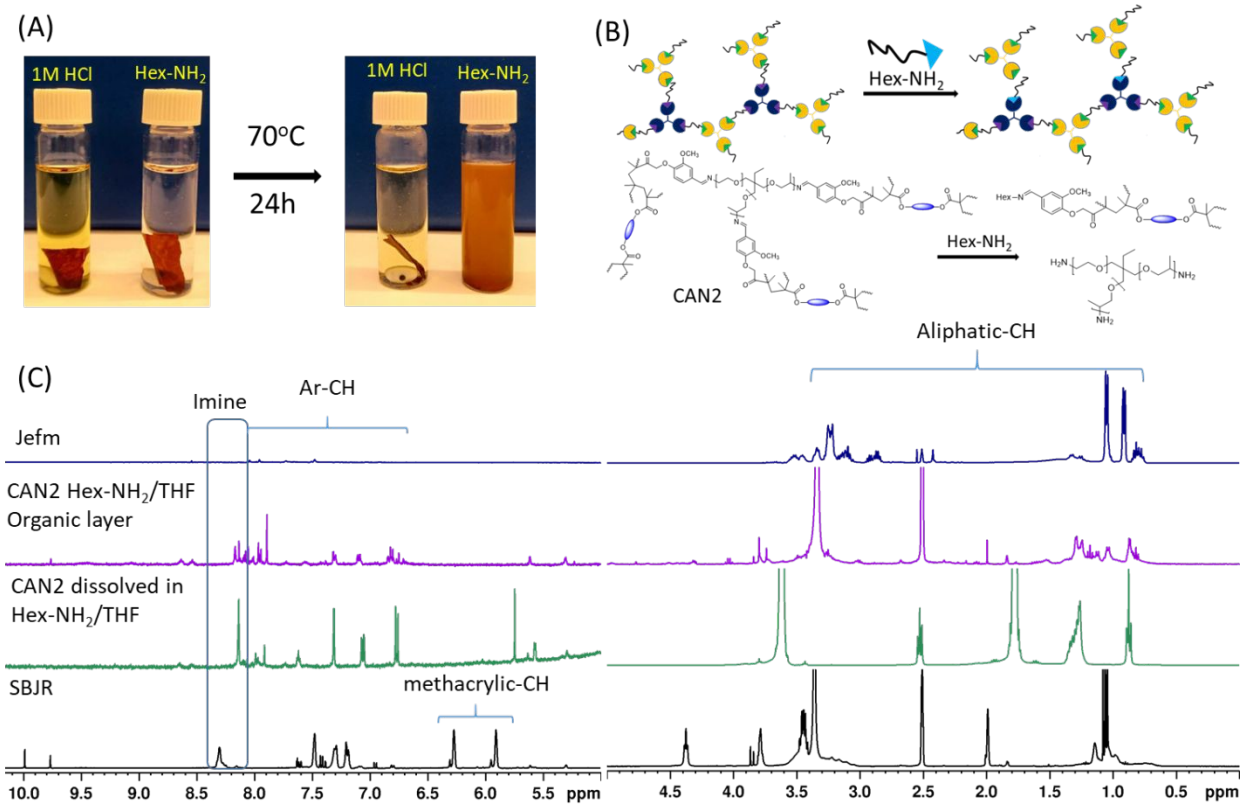

Figure 5. (A) Chemical degradation attempt of CAN2 with 1M HCl or hexylamine/THF solution, (B) the proposed reaction mechanism for chemical degradation of CAN2 by hexylamine/THF, and (C) ^{1}H NMR (400.13 Hz, DMSO-d_6) spectra of SBJR resin, crude product of CAN2 dissolved in hexylamine/THF, organic layer after extraction with ethyl acetate.

Conclusions

Post-consumer PET bottles and PBT fabrics were successfully transformed into highly-reactive photocurable resins and dynamic covalent networks. The synthesis of PET and PBT derived resins (PR, FR), and a Schiff-base resin (SBJR), along with their integration into two permanently crosslinked thermosets and two CANs, highlights the versatility of the approach and its potential to support more circular polymer design. Structural analysis by NMR and FTIR

View Article Online
DOI: 10.1039/D6PY00244G

confirmed the targeted chemical transformations, while thermal analysis supported very good thermal stability after curing. The CAN1 and CAN2, containing imine-based exchangeable bonds, exhibited dynamic behavior at elevated temperatures while maintaining associative network characteristics. While CAN2 could be thermally reprocessed to good quality films, reprocessing of CAN1 resulted in fragile material. In spite of the resistance to degradation under commonly reported acidic conditions, the materials remained chemically degradable through transimination, allowing targeted depolymerization to recover resin components such as Jeffamine. Overall, the materials developed in this work combine recycled feedstocks, photocurability, thermal robustness, reprocessability, and selective chemical degradability. The demonstrated recycling pathways underscore the potential for integrating dynamic covalent chemistry into waste-derived polymer systems to advance material circularity. However, further research is needed to optimize processes and to assess the long-term performance, scalability, and overall environmental impact.

Author Contributions

Sathiyaraj Subramaniyan contributed to conceptualization and wrote the original draft. Sathiyaraj Subramaniyan, Amro Hindi and Federico Guerrero-Ruiz performed the experimental work, analysis of results and data curation. Minna Hakkarainen conceptualized and supervised the work, reviewed and edited the final manuscript.

Conflicts of interest

The authors declare no competing financial interest.

Acknowledgments

This work was partially supported by the Wallenberg Initiative Materials Science for Sustainability (WISE) funded by the Knut and Alice Wallenberg Foundation.

View Article Online
DOI: 10.1039/D6PY00244G

References

1. A. M. Al-Sabagh, F. Z. Yehia, G. Eshaq, A. M. Rabie and A. E. Elmetwally, *Egypt. J. Pet.*, 2016, **25**, 53–64.
2. Z. Liu, H. Zhang, S. Liu and X. Wang, *Polym. Chem.*, 2023, **14**, 1110–1116.
3. R. Carmenini, A. S. De León, T. Benelli, L. Giorgini, M. C. Franchini, S. I. Molina and M. Maturi, *Macromol. Rapid Commun.*, 2025, **27**, 12830–12843.
4. M. Y. Suleman, H. L. Judah, P. Bexis, P. Fennell, J. P. Hallett and A. Brandt-Talbot, *Green Chem.*, 2025, **27**, 11475–11490.
5. K. Kaiser, M. Schmid and M. Schlummer, *Recycling*, 2018, **3**, 1.
6. S. Singh and R. Sarkar, *Polym. Chem.*, 2025, **16**, 4870–4880.
7. S. V. Pandeirada, P. S. S. Lacerda and M. A. R. Meier, *Green Chem.*, 2025, **28**, 2706-2714.
8. K. Ghosal and C. Nayak, *Mater. Adv.*, 2022, **3**, 1974–1992,
9. E. Lorusso, N. Parasothy, Y. Feng, J. Schneider, L. Kamps, T. Mayer-Gall, J. S. Gutmann and W. Ali, *J. Appl. Polym. Sci.*, 2022, **3**, 594–607.
10. S. Feng, J. Xie, Y. Ding, C. Yan and F. Yan, *Chem. Mater.*, 2025, **37**, 6667−6677.
11. I. Olazabal, E. J. L. Barrios, S. De Meester, C. Jehanno and H. Sardon, *ACS Appl. Polym. Mater.*, 2024, **6**, 4226–4232.
12. Y. Chen, P. Ranganathan, Y. Lee and S. Rwei, *ACS Sustainable Chem. Eng.*, 2021, **9**, 3518-3528.
13. G. P. Karayannidis and D. S. Achilias, *Macromol. Mater. Eng.*, 2007, **292**, 128–146,
14. B. Eva, Ö. Ckström and M. Hakkarainen, *Eur. Polym. J.*, 2021, **151**, 110441.
15. M. Hakkarainen, N. Kasmi and B. Eva, *Resour. Conserv. Recycl.*, 2023, **193**, 106974.

View Article Online
DOI: 10.1039/D6PY00244G

16. S. Shirazimoghaddam, I. Amin, J. A. F. Albanese and N. R. Shiju, *ACS Eng. Au*, 2023, **3**, 37-44.

17. Y. Peng, J. Yang, C. Deng, J. Deng, L. Shen and Y. Fu, *Nat. Commun.*, 2023, **14**, 3249.

18. S. Subramaniyan, N. Najjarzadeh, S. R. Vanga, A. Liguori, P. Syr and M. Hakkarainen, *ACS Sustainable Chem. Eng.*, 2023, **11**, 3451-3465.

19. E. Rusen, A. Mocanu, O. Brincoveanu, G. Toader, A. Diacon, M. Aldrigo, G. Ciuprina and C. Romanit, *ACS Sustainable Resour. Manage.*, 2025, 11, 2292-2301.

20. Z. Liu, S. Liu and X. Wang, *J. Mater. Chem. A*, 2024, **12**, 9454–9461.

21. D. Jia, L. Li, Y. Yang, J. Zhang, T. Yang, H. Lin, H. Huang and G. Zhong, *Macromolecules*, 2025, **58**, 9504-9514.

22. M. Kim and I. Ro, *Chem. Commun.*, 2025, 61, 19390–19402.

23. N. V. Reis, Y. Zhou, B. Bati, Y. Wang, G. S. Nichol, J. A. Garden and A. P. Dove, *J. Am. Chem. Soc.*, 2025, 147, 36697–36705.

24. B. T. Nguyen, T. T. Y. Tan, K. Otake, S. Kitagawa and J. Y. C. Lim, *Angew. Chem. Int. Ed.*, 2025, **64**, 202504017.

25. Y. Ogiwara and K. Nomura, *ACS Org. Inorg. Au*, 2023, **3**, 377-383.

26. N. Markandeya, B. S. Solanki, K. Ramalingam and S. Kamble, *Ind. Eng. Chem. Res.*, 2025, 64, 16428–16441.

27. S. Javed, J. Fisse and D. Vogt, Polymers, 2023, **15**, 687 2023.

28. Y. Wang, Y. Zhang, H. Song, Y. Wang, T. Deng and X. Hou, *J. Clean. Prod.*, 2019, **208**, 1469–1475.

29. A. M. Al-Sabagh, F. Z. Yehia, A. M. F. Eissa, M. E. Moustafa, G. Eshaq, A. M. Rabie and A. E. Elmetwally, *Polym. Degrad. Stab.*, 2014, **110**, 364–377.

View Article Online
DOI: 10.1039/D6PY00244G

30. F. Li, X. Yao, R. Ding, Y. Bao, Q. Zhou, D. Yan, Y. Li, J. Xu, J. Xin and X. Lu, *Green Chem.*, 2024, **26**, 9802–9813.

31. G. Ha, A. Mamunur, J. Ha and C. Yoo, *Chemosphere*, 2024, **349**, 140781.

32. O. A. Attallah, A. Janssens, M. Azeem and M. B. Fournet, *ACS Sustainable Chem. Eng.*, 2021, 9, 17174–17185.

33. A. Liguori, S. Subramaniyan, J. G. Yao and M. Hakkarainen, *Eur. Polym. J.*, 2022, **178**, 111489.

34. S. Ghosh, S. Subramaniyan, A. Bisht and B. Nandan, *J. Mater. Chem. B*, 2025, **13**, 2352–2365.

35. S. Subramaniyan, B. Zhang and P. Syr, *Chem. Eng. J.*, 2024, **501**, 157632.

36. N. Zheng, Y. Xu, Q. Zhao and T. Xie, *Chem. Rev.*, 2021, **121**, 1716–1745.

37. K. Odelius, *Biomacromolecules*, 2024, **25**, 2348–2357.

38. S. Zhao and M. M. Abu-Omar, *Macromolecules*, 2018, **51**, 9816–9824.

(39) Zhou, Y.; Goossens, J. G. P.; Sijbesma, R. P.; Heuts, J. P. A. *Macromolecules*, 2017. **50**, 6742−6751.

(40) Demongeot, A.; Groote, R.; Goossens, H.; Hoeks, T.; Leibler, L. *Macromolecules*, 2017, **50**, 6117−6127.

(41) Qiu, J.; Ma, S.; Wang, S.; Tang, Z.; Li, Q.; Tian, A.; Xu, X.; Wang, B.; Lu, N.; Zhu, J. *Macromolecules*, 2021, **54**, 703-712.

(42) F. Gholami, M. Li, A. Hucker, S. Clark, K. Zhou and H. J. Qi, *ACS Appl. Polym. Mater.*, 2025, **7**, 16194−16205.

(43) Y. Xu, K. Odelius and M. Hakkarainen, *ACS Sustainable Chem. Eng.*, 2020, 46, 17272–

View Article Online
DOI: 10.1039/D6PY00244G

17279.

(44) S. Ügdüler, K. M. Van Geem, R. Denolf, M. Roosen, N. Mys, K. Ragaert and S. De Meester, *Green Chem.*, 2020, **22**, 5376–5394.

Data availability statement

View Article Online
DOI: 10.1039/D6PY00244G

All data required to understand and verify the research results is available as part of the main article or in the supplementary information.